Research Paper

Finite Element Modelling of a Flow-Acoustic Coupling in Unbounded Domains

Paweł ŁOJEK*, Ireneusz CZAJKA, Andrzej GOŁAŚ

AGH – University of Science and Technology
Department of Power Systems and Environmental Protection Facilities
Kraków, Poland
*Corresponding Author e-mail: lojek@agh.edu.pl

One of the main issues of design process of HVAC systems and ventilation ducts in particular is correct modelling of coupling of the flow field and acoustic field of the air flowing in such systems. Such a coupling can be modelled in many ways, one of them is using linearised Euler equations (LEE). In this paper, the method of solving these equations using finite element method and open source tools is decribed. Equations were transformed into functional and solved using Python language and FEniCS software. The non-reflective boundary condition called buffer layer was also implemented into equations, which allowed modelling of unbounded domains. The issue, influence of flow on wave propagation, could be adressed using LEE equations, as they take non-uniform mean flow into account. The developed tool was verified and results of simulations were compared with analytical solutions, both in one- and two-dimensional cases. The obtained numerical results are very consistent with analytical ones. Furthermore, this paper describes the use of the developed tool for analysing a more complex model. Acoustic wave propagation for the backward-facing step in the presence of flow calculated using Navier-Stokes equations was studied.

Keywords: linearised Euler equations (LEE); FEniCS; finite element method; non-reflective boundary conditions; open source.

1. Introduction

When using HVAC systems in buildings, acoustic comfort is one of the crucial features from the user's point of view. One of the main factors affecting acoustic comfort is ambient noise caused in modern buildings by components of HVAC systems, such as fans, ventilation units, and air conditioning systems. The noise that is produced by these devices could be further enhanced by air ducts. Understanding the behaviour of acoustic wave in the presence of the flow in ducts is important in the design and operation of such systems. It requires experimental or numerical analysis, of which the latter is more often used, because of economical reasons.

The most widely used model for the behaviour of the fluid and the acoustic wave are Navier-Stokes equations. However, using them involves many problems resulting from the lack of their exact solution for the general case (WAGNER *et al.*, 2006). The most accurate method is direct numerical simulation (DNS) of the equations, which provides a full picture of the phenomena, associated with both the flow of fluid and the propagation of the wave. However, according to (COLONIUS, 1997), the computational complexity of the DNS method is too large to be used in engineering applications. Computational aeroacoustic (CAA) methods are often used for this purpose. The classical approach is to use large eddy simulation (LES) method, which is less accurate (and computationally complex) than DNS, to compute the fluid flow. Then, acoustic analogies are used to calculate the sound pressure level in the far field (WAGNER *et al.*, 2006). Most of the acoustic analogies are based on the acoustic analogy derived by LIGHTHILL (1952). The disadvantage of this method is the lack of information about phenomena occurring in the near field. This classical, hybrid approach is implemented in state-of-the-art numerical software, such as Actran, ANSYS Fluent, Comsol, or OpenFOAM (EPIKHIN *et al.*, 2015). An alternative method used for computational aeroacoustics is called Kirchoff's integral method. It consists of calculating the nonlinear near (flow) field using Navier-Stokes equations and then using Kirchhoff sur-

face integral to find the acoustic pressures at far field (LYRINTZIS, GEORGE, 1989).

Another hybrid method is to use Navier-Stokes equations to simulate the fluid flow, and then couple the fluid velocity field described by them with acoustic field described by one of the propagation models. The most used acoustic propagation models are well known linearised Euler equations (LEE) described for example in (BAILLY, JUVÉ, 2000) and acoustic perturbation equations proposed by (EWERT, SCHRÖDER, 2003). In this paper, this modelling approach was used. Acoustic propagation model given by linearised Euler equations was used in combination with Navier-Stokes equations. From the mathematical point of view, linearised Euler equations are a system of partial differential equations. The exact solution of the equations are known only for basic, one or two-dimensional cases. For more complex cases and geometries, approximate methods, such as finite element (FEM), difference (FDM), and volume (FVM) methods are commonly used. The paper proposes the implementation of solver for linearised Euler equations in Python using the finite element software FEniCS (ALNAES *et al.*, 2015). Linearised Euler equations in the form which takes the non-uniform velocity field into account were implemented, which ultimately allowed describing the coupling of flow and acoustic fields. This represents the suitability of the tool for modelling the behaviour of HVAC systems and air in ducts. In order for created tool to be used more widely, for modelling unbounded domains, it was necessary to propose and implement a non-reflecting boundary condition. A buffer zone condition has been selected for this purpose.

The created tool has been tested and verified in two test cases for which analytical solution is known. It was then used to calculate the behaviour of a sinusoidal acoustic wave in the presence of a non-uniform flow, calculated using the Navier-Stokes equations. The chosen geometric model for these simulations is a well known and researched backward-facing step. This geometry can be used to model, for example, channel discontinuity.

FEniCS software was chosen due to the fact that it is open source software, easy to use from a programming point of view, and allowing connection with pre- and post-processing tools. Due to its structure and workflow, FEniCS allows to focus on the parts of mathematical and physical modelling, it is not necessary to go into the details of the implementation of FEM. For pre-processing, i.e. geometry and mesh generation, the Salome software was used (RIBES, CAREMOLI, 2007). The post-processing of the results was performed using self-developed Python scripts and Paraview tool (AHRENS *et al.*, 2005). Paraview was also used for visualisation of results.

2. Mathematical model

Continuity (1) and Navier-Stokes (2) equations are mainly used to describe the behaviour of the fluid (RIENSTRA, HIRSCHBERG, 2004):

$$\frac{\partial \rho}{\partial t} + \frac{\partial \rho v_i}{\partial x_i} = 0, \tag{1}$$

$$\rho \frac{\partial v_i}{\partial t} + \frac{\partial P_{ji}}{\partial x_j} + \rho v_j \frac{\partial v_i}{\partial x_j} = f_i, \tag{2}$$

where p is the pressure, v_i is the velocity, t is the time, ρ is the density, f_i is the external force density, $P_{ij} = p\delta_{ij} - \tau_{ij}$ is the fluid stress tensor, τ_{ij} is the viscous stress tensor, $i, j = 1, 2, 3$ are dimensions.

Euler equations can be derived from Navier-Stokes equations by the assumption of inviscid and homoentropic flow (ÅBOM, 2006; MECHEL, 2008):

$$\frac{\partial \rho}{\partial t} + \frac{\partial \rho v_i}{\partial x} = 0, \tag{3}$$

$$\frac{\partial \rho v_i}{\partial t} + \frac{\partial}{\partial x_j} \left(\rho v_i v_j + p\delta_{ij} \right) = 0. \tag{4}$$

Equations can be linearised around the mean value of the parameters describing the flow, such as pressure, density, or velocity. This allows to obtain linearised Euler equations which allow determining acoustic wave propagation (RIENSTRA, HIRSCHBERG, 2004).

Assuming that each variable describing the flow can be divided into a mean and acoustic component, it can be written (DYKAS *et al.*, 2010):

$$p = \overline{p} + p', \qquad v_i = \overline{v_i} + v_i', \qquad \rho = \overline{\rho} + \rho', \tag{5}$$

where $\overline{p}, \overline{v}, \overline{\rho}$ are mean variables, p', v_i', ρ' are acoustic variables (pressure, velocity in i-th direction, density).

Inserting the above into the equations (3) and (4), assuming the mean values $\overline{p}, \overline{v_i} = 0, \overline{\rho} = \text{const}$ and using ideal gas equation of state given by:

$$p' = c^2 \rho' \tag{6}$$

allows to derive linearised Euler equations which describes acoustic wave propagation without a mean flow. The equations are written below:

$$\frac{\partial p'}{\partial t} + c^2 \overline{\rho} \frac{\partial v_j'}{\partial x_j} = 0, \tag{7}$$

$$\overline{\rho} \frac{\partial v_i'}{\partial t} + \frac{\partial p'}{\partial x_i} = 0, \tag{8}$$

Linearised Euler equations can be reduced to the classic wave equation by taking the time derivative of Eq. (7), divergence of Eq. (8), and combining them (RIENSTRA, HIRSCHBERG, 2004):

$$\frac{\partial^2 p'}{\partial t^2} - \frac{1}{c^2} \frac{\partial^2 p'}{\partial x_i^2} = 0. \tag{9}$$

2.1. Non-uniform mean flow

Equations (7) and (8) allow for description of wave propagation without a mean flow. If the derivation assumes the presence of mean velocity distribution $\overline{v_i}$, equations take on a more complex form.

In one-dimensional case equations take the form $(v_1' = u, \overline{v_1} = U, p' = p, \overline{p} = 0, x_1 = x)$:

$$\frac{\partial p'}{\partial t} = -\overline{\rho}c^2\frac{\partial u}{\partial x} - U\frac{\partial p}{\partial x} - p\frac{\partial U}{\partial x}, \tag{10}$$

$$\frac{\partial u}{\partial t} = -\frac{1}{\overline{\rho}}\frac{\partial p}{\partial x} - U\frac{\partial u}{\partial x} - u\frac{\partial U}{\partial x} - \frac{pU}{c^2\overline{\rho}}\frac{\partial U}{\partial x}, \tag{11}$$

while in two-dimensional case $(v_1' = u, v_2' = v, \overline{v_1} = U, \overline{v_2} = V, p' = p, \overline{p} = 0, x_1 = x, x_2 = y)$ (Povitsky, 2000):

$$\frac{\partial p}{\partial t} = -\overline{\rho}c^2\left(\frac{\partial u}{\partial x} + \frac{\partial v}{\partial y}\right) - U\frac{\partial p}{\partial x} - V\frac{\partial p}{\partial y}$$
$$-p\left(\frac{\partial U}{\partial x} + \frac{\partial V}{\partial y}\right), \tag{12}$$

$$\frac{\partial u}{\partial t} = -\frac{1}{\overline{\rho}}\frac{\partial p}{\partial x} - U\frac{\partial u}{\partial x} - u\frac{\partial U}{\partial x} - V\frac{\partial u}{\partial y} - v\frac{\partial U}{\partial y}$$
$$-\frac{p}{\overline{\rho}c^2}\left(U\frac{\partial U}{\partial x} + V\frac{\partial U}{\partial y}\right), \tag{13}$$

$$\frac{\partial v}{\partial t} = -\frac{1}{\overline{\rho}}\frac{\partial p}{\partial y} - V\frac{\partial v}{\partial y} - v\frac{\partial V}{\partial y} - U\frac{\partial v}{\partial x} - u\frac{\partial V}{\partial x}$$
$$-\frac{p}{\overline{\rho}c^2}\left(U\frac{\partial V}{\partial x} + V\frac{\partial V}{\partial y}\right). \tag{14}$$

For the purpose of solving these equations with the FEniCS software, they had to be discretised in time and written in the variational form.

2.2. Boundary conditions

System of linearised Euler equations is an example of an initial-boundary value problem. Initial and boundary conditions have to be provided in the case to solve the equations. Initial conditions describe pressure and velocity distribution in computational domain at the beginning of simulations, and boundary conditions describe pressure and velocity on boundaries. While initial conditions differ depending on the case being solved, in a general case several types of boundary conditions can be distinguished, such as Dirichlet, Neumann, and Robin boundary conditions.

In the case of acoustical simulations, the following boundary conditions can be defined (Kaltenbacher, 2017):

- acoustically hard boundary – this assumes that acoustic impedance of wall approaches infinity, the wave is fully reflected from the boundary, Neumann boundary condition can be derived from the linearised Euler Eq. (8):

$$\boldsymbol{n} \cdot \nabla p' = \frac{\partial p'}{\partial \boldsymbol{n}} = 0; \tag{15}$$

- non-reflective boundary – the wave is damped/absorbed, the definition of non-reflective boundary condition is more complicated and cannot be reduced to simple Dirichlet or Neumann conditions.

The main purpose of non-reflective boundary condition (NRBC) is to mimic unlimited physical domain in bounded numerical domain. It can be done in many ways, including characteristic NRBC (Giles, 1990; Atkins, Casper, 1994; Koloszár *et al.*, 2019), radiation boundary condition (Hagstrom, Goodrich, 2003), absorbing boundary conditions (Givoli, 2008; Kosloff, Kosloff, 1986), not to mention Perfectly Matched Layer (Berenger, 1994; Bermudez *et al.*, 2008).

In this work, absorbing boundary condition called buffer layer (zone), which was described in e.g. (Richards *et al.*, 2004; Gill *et al.*, 2017). The method was chosen for its simplicity, efficiency, and ease of implementation in FEniCS, contrary to the Perfectly Matched Layer.

The buffer layer is introduced into the governing equations by adding a damping term as follows:

$$\frac{\partial \phi}{\partial t} = L(\phi) + \sigma(x_i)\phi, \tag{16}$$

where ϕ is the flow variable, $L(\phi)$ is the spatial operator, $\sigma(x_i)$ is the damping term.

The boundary condition, described in greater detail in (Richards *et al.*, 2004; Gill *et al.*, 2017), was transformed to the form that could be implemented in FEniCS software and was written as a piecewise function:

$$\sigma(x) = \begin{cases} -\alpha\left(1 - \dfrac{x}{L}\right)^{\beta} & x > L, \\ 0, & x < L, \end{cases} \tag{17}$$

where α is the strength of damping, L is the start of the buffer zone, β is the shape of the damping curve.

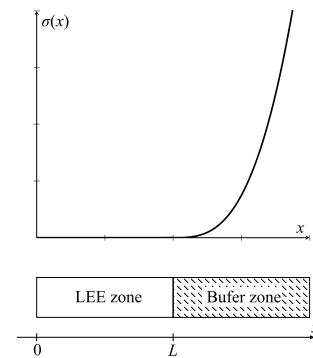The working principle of the implemented boundary condition is shown in Fig. 1.

Fig. 1. Example of one-dimensional buffer zone with a corresponding σ function (Łojek, Czajka, 2019).

2.3. Numerical methods

2.3.1. Temporal discretisation

The solved equations had to be discretised in time due to the fact that the wave propagation phenomenon is transient.

The Adams-Moulton method of the fist order was used for this purpose. Described in more detail in (Butcher, 2016; Czajka, Gołaś, 2017), the method allows for approximation of differential equation in the form:

$$\frac{\partial x}{\partial t} = f(x,t), \qquad x(t=0) = x_0, \qquad (18)$$

in the next timesteps by:

$$x^{[n+1]} = x^{[n]} + \Delta t f\left(x^{[n+1]}, t^{n+1}\right), \qquad (19)$$

where $x(t_n) = x^{[n]}$, $x(t_{n+1}) = x^{[n+1]}$, $\Delta t = t_{n+1} - t_n$.

Despite the simplicity of the method, it can be shown that it is L-stable and sufficient for the purposes of this study (Czajka, Gołaś, 2017).

2.3.2. Finite element method in FEniCS software

FEniCS software uses the finite element method for solving the equations. It is based on Galerkin method and Lax-Milgram theorem, assuming the existence of a unique solution to the variational problem (Logg *et al.*, 2012).

The algorhitm of solving equation in FEniCS consists of:

- writing the equation in variational formulation:

$$a(u,v) = L(v) \quad \text{for all} \quad v \in \widehat{V}, \qquad (20)$$

  where v is the test function, u is the trial function, $\widehat{V}$, V are test and trial function spaces, $a(u,v)$ is the bilinear form, $L(v)$ is the linear form,

- spatial discretisation of the equations:

$$a(u_h,v) = L(v) \quad \text{for all} \quad v \in \widehat{V_h}, \qquad (21)$$

  where $\widehat{V_h} \subset \widehat{V}$, $V_h \subset V$ are discrete test and trial function spaces,

- solving the system of linear equations:

$$AU = b, \qquad (22)$$

  where $A_{ij} = a(\phi_i \widehat{\phi}_j)$, $b_i = L(\widehat{\phi}_i)$, and ϕ, $\widehat{\phi}$ are basis functions for discrete trial and test spaces V, $\widehat{V}$.

Linearised Euler equations discretised in time and space had to be derived to solve them using FEniCS, which is shown below:

$$\int_\Omega p'^{[n+1]}q \, dx - \int_\Omega p'^{[n]}q \, dx + \Delta t c^2 \bar{\rho} \int_\Omega \nabla \cdot u_i'^{[n+1]}q \, dx$$

$$+ \sigma(x) \int_\Omega p'^{[n+1]}q \, dx = 0 \quad \text{in} \quad \Omega, \qquad (23)$$

$$\int_\Omega v_i'^{[n+1]}w \, dx - \int_\Omega v_i'^{[n]}w \, dx + \frac{\Delta t}{\bar{\rho}} \int_\Omega \nabla p'^{[n+1]}w \, dx$$

$$+ \sigma(x) \int_\Omega u'^{[n+1]}_i w \, dx = 0 \quad \text{in} \quad \Omega. \qquad (24)$$

Only Eqs (7) and (8) (without the mean flow) are shown in variational form, because of their simplicity, compared to Eqs (10) and (11) (one-dimensional case) or Eqs (12)–(14) (two-dimensional case), which describes propagation with the mean flow velocity. All of these equations were implemented in FEniCS software.

3. Validation of the model

To verify the adopted model, a series of calculations were performed:

- modelling of wave propagation in one-dimension with and without the presence of the mean flow;

- modelling of pulse propagation in a two-dimensional rectangular domain without the mean flow and with uniform and non-uniform mean velocity fields;

- model of wave propagation from oscillating cylinder, without the presence of the mean flow;

- model of backward-facing step without and with the mean velocity field calculated using Navier-Stokes equations.

The description and results of each case are presented below. If possible, the results of the computations were compared to analytical ones.

3.1. One-dimensional propagation

In the first case, propagation of an acoustic wave with a sinusoidal excitation (pressure Dirichlet boundary condition) at one of the boundaries was tested. The purpose of one-dimensional modelling was to check if the correct mathematical model was adopted and whether the implemented boundary condition could be used for acoustic simulations.

The values of pressure at the boundary ($x = 0$) were described by Eq. (25):

$$p'(t) = A\sin(2\pi f t). \qquad (25)$$

The modelling results with no mean flow velocity taken into account were compared to the analytical solution, given by:

$$p'(x,t) = \sin(kx + 2\pi f t t). \qquad (26)$$

The effect of mean velocity on the acoustic wave was checked using a simple Doppler model, given by Eq. (27) (Kuttruff, 2007). It was checked whether

there was a change of frequency caused by mean velocity

$$f' = \left(1 + \frac{V}{c}\right)f, \qquad (27)$$

where V is the relative velocity between the listener and the source.

In addition, the behaviour of the damping zone described by Eq. (17) was checked. The coefficients $\alpha = 5$ and $\beta = 3$ were assumed as damping function parameters. In the calculations, 20 elements were assumed per one wavelength. The amplitude of pressure at boundary was equal to 5 Pa. Timestep Δt for all one-dimensional simulations was equal to 10^{-5} s, and simulation time $T = 0.02$ s was assumed. Speed of sound c equal to 340 m/s and air density ρ equal to 1.2 kg/m^3 were adopted.

Firstly, compliance of results with analytical formulas was checked. The model showed great agreement with them. In addition, according to the assumptions, the wave was completely damped in the buffer zone. For each given excitation frequency, the propagation of acoustic wave was well mapped compared to the analytical formula.

The root mean square error was also computed. It is given by an equation (BENDAT, PIERSOL, 2010):

$$\text{RMSE}\,(\widehat{\phi}) = \sqrt{E\left[(\widehat{\phi} - \phi)^2\right]}, \qquad (28)$$

where $\widehat{\phi}$ is the estimator of ϕ (simulation results), ϕ are the analytical results. The results for range of pressure excitation frequencies at the left boundary were shown in the Fig. 2. The results of the analysis for given frequencies were shown in Table 1.
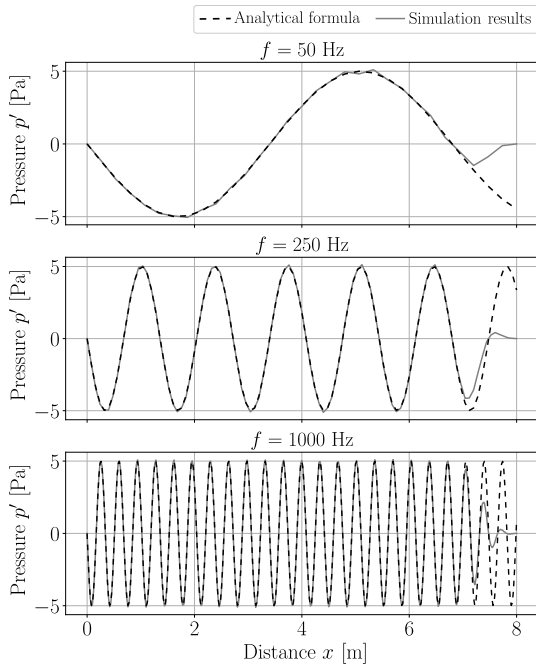
Table 1. Root mean square error
for data shown in Fig. 2.

Frequency [Hz]	RMSE
50	0.1472
150	0.1103
250	0.0939
500	0.0747
1000	0.0682
2000	0.0754

In the same way, mesh independency was analysed for given excitation frequency, 340 Hz, for which wavelength λ is equal to 1 m. It was examined how the accuracy of the solution changes depending on the number of elements per wavelength. The results are shown in Fig. 3 and in Table 2. For 6.25 elements per wavelength, the results are starting to lose accuracy. However, they do not differ significantly from the analytical results. For 2.5 and fewer elements per wavelength the results are inaccurate and poorly reproduce the behaviour of the wave.
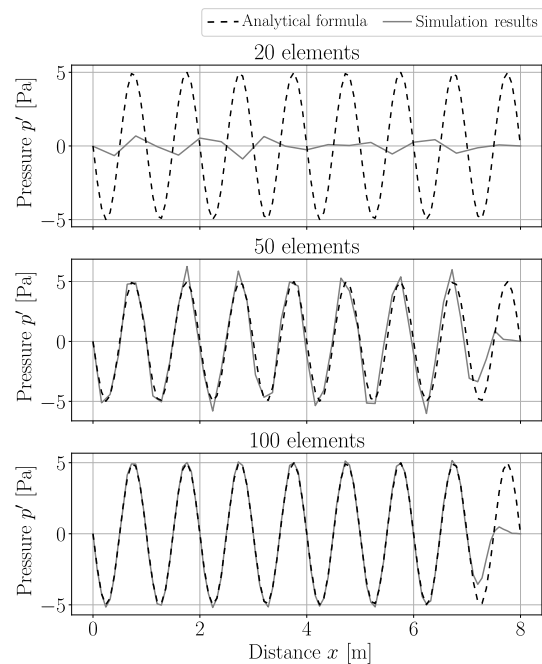

Fig. 3. Mesh independence study for one-dimensional case.

Table 2. Root mean square error for mesh independence study (Fig. 3).

Elements	Elements per wavelenght	RMSE
20	2.50	3.3089
50	6.25	0.8456
100	12.50	0.1351
250	31.25	0.0226
500	62.60	0.0057
1000	125.00	0.0017

Fig. 2. Comparison of analytical and simulation results for one-dimensional propagation of sine wave.

It was also checked how constant mean velocity affects the wave frequency. Again, the selected wave frequency was equal to $f = 340$ Hz. In these simulations, the time step has to be reduced to $\Delta t = 10^{-6}$ s. The error metric was Doppler effect Eq. (27); frequency change caused by velocity was compared with the analytical Doppler effect equation frequency. Relative error was computed using Eq. (29):

$$\delta f = \left| \frac{f_D - \frac{f_1 + f_2}{2}}{f_D} \right|. \tag{29}$$

The changed frequency was calculated on the basis of wavelength measured at two points in the manner such as shown in Fig. 4. The mean velocity used in the calculations was assumed as the relative velocity of the source and the listener in Eq. (27). The results are pre-

sented in Fig. 5 and in Table 3. In Fig. 5, it can be seen that the mean velocity affects the acoustic wave. Depending on the direction of velocity, the wavelength is reduced or extended as intended.
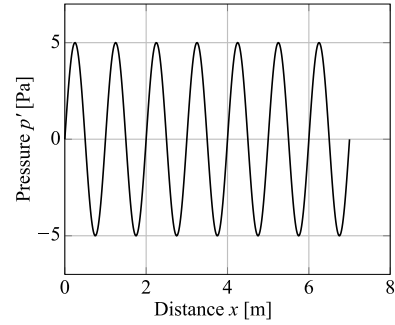
Fig. 4. Measured wavelengths.
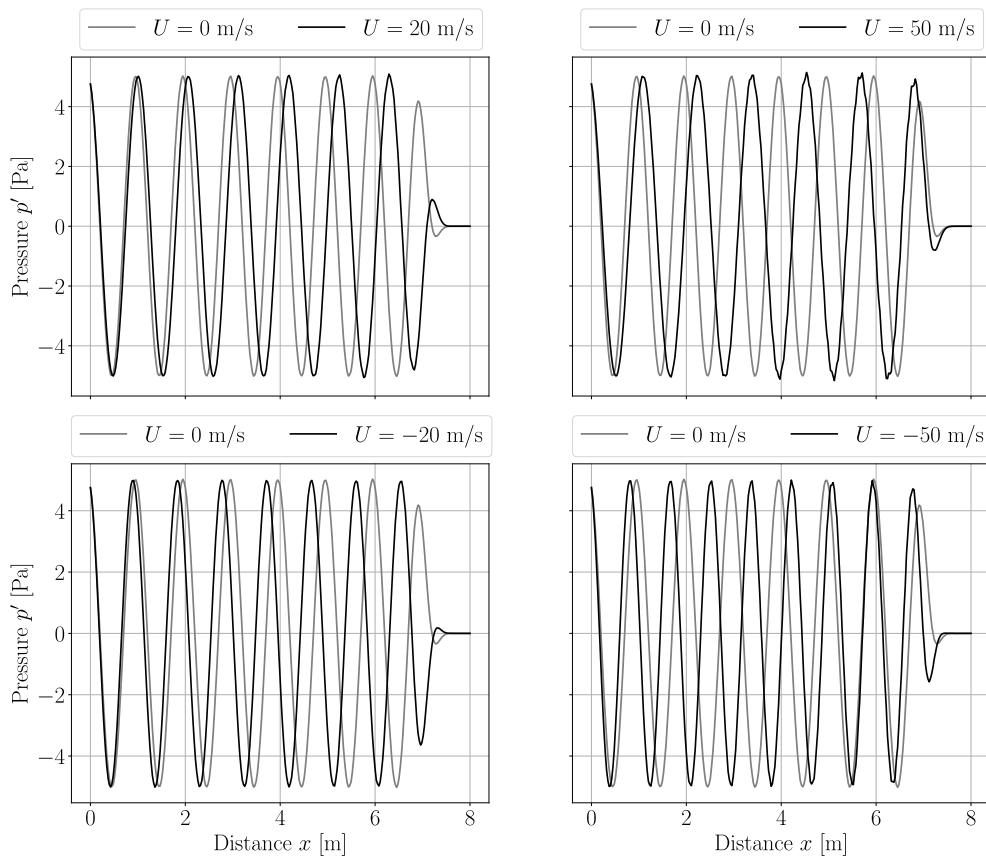
Fig. 5. Results of the simulations with a uniform mean flow velocity.

Table 3. Results of the simulations with a uniform mean velocity (Fig. 5).

U [m/s]	λ_1 [m]	λ_2 [m]	f_1 [Hz]	f_2 [Hz]	f_D [Hz]	Rel. error [%]
20	1.052	1.055	323.2	322.3	320	0.85
−20	0.925	0.927	367.6	366.8	360	2.00
50	1.152	1.184	295.1	287.2	290	−0.38
−50	0.830	0.832	409.6	408.2	390	−4.90

3.2. Two-dimensional pulse

In the two-dimensional case, propagation of pulse given by Eq. (30) in rectangular domain was analysed. Initial distribution of pressure and dimensions of the domain were shown in Fig. 6. The computational domain was a grid made of 400×400 nodes. Thickness of the buffer zone introduced to attenuate the acoustic wave on boundaries was equal to 4 m

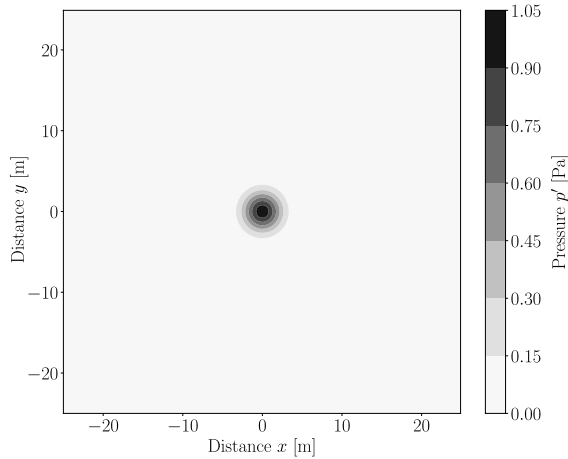$$p'(x,y,t)_{t=0} = \exp\left(-\ln(2)\frac{x^2 + y^2}{2}\right). \quad (30)$$

Fig. 6. Initial values of pressure in the two-dimensional case.

For the initial pulse given by Eq. (30), analytical solution is known and given by the equation (Dykas, Wroblewski, 2006):

$$p'(x,t) = \frac{\epsilon}{2\alpha} \int_0^\infty \left(\xi \exp\left(\frac{-\xi^2}{(4\alpha)}\right)\cos(at\xi)J_0(\xi\eta)\right)d\xi, \quad (31)$$

where $\eta = \sqrt{(x-Mt)^2 + y^2}$, $\alpha = \ln(2)/b^2$, $\epsilon = 0.03$, $b = 5$ are constants, J_0 is the Bessel function of the first kind.

At first, the behaviour of the buffer zone without the mean flow was checked. The values of pressure along x axis for $y = 0$ for various times were shown in Fig. 7.

It can be seen that the results mostly coincide with the analytical distribution described by Eq. (31), which proves the correctness of the implementation of the adopted model. The main differences between the numerical and analytical results appear for times greater than $t = 0.08$ s, when the reflection occurs. In the case without the buffer zone, the wave is reflected from the boundary. When the buffer zone is used, the wave is fully attenuated. The difference between numerical results for the buffer zone case and analytical results is due to the way boundary condition is defined. In simulations, the values of pressure at the edges of computational domain were equal to 0, and in Eq. (31), the boundary is assumed at infinity. However, it should be noted that near the centre of the
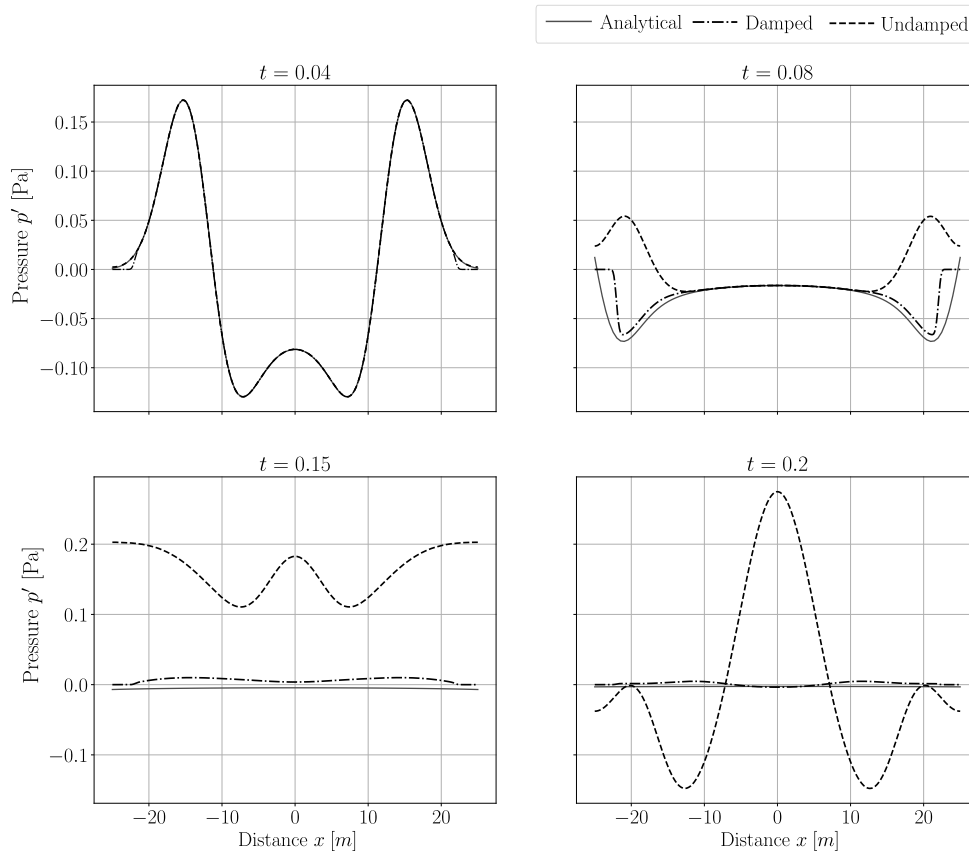

Fig. 7. Distribution of pressure along x axis for $y = 0$ for simulations of two-dimensional impulse (without the mean flow).

domain the results do not differ from one another, and with increasing of simulation time, they would converge. Increasing the number of elements and reducing the time step could also affect the accuracy of the solution.

Next, the simulation and solver behaviour was checked in the presence of a non-uniform mean flow. Two cases were investigated for the same computational domain as before. In the first one, the velocity field had a uniform distribution and was equal to 50 m/s. In the second one, the influence of the shear flow was investigated. The velocity was given by equation:

$$U(x,y) = 40\sin\left(\frac{x}{\frac{\pi}{4}}\right) \tag{32}$$

and was shown in Fig. 8.

The distribution of pressure compared to cases without a flow was shown in Fig. 9. The results for the damped case only were shown. In Figs 9, it can be seen that when the mean flow is constant, the wave is shifted in the direction of the flow. For the mean flow given by Eq. (32) the pressure distribution is comparable to the analytical one, as expected (the mean velocity for $y = 0$ is equal to 0 m/s).

For all cases without absorbing the boundary condition, the wave bounces off the hard walls and further
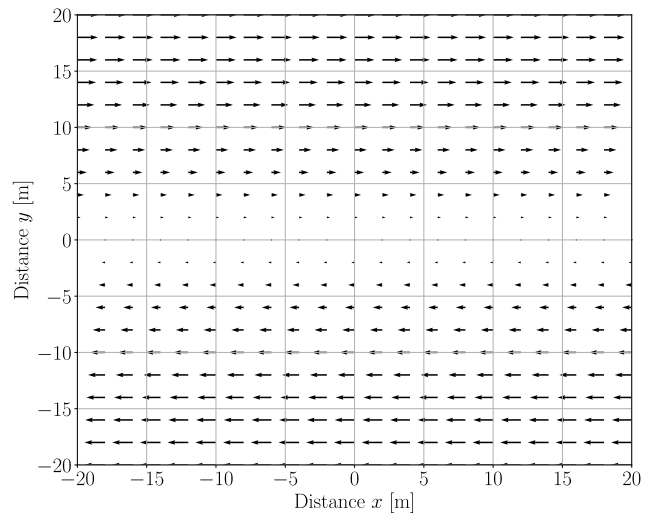

Fig. 8. Distribution of the shear flow mean velocity given by Eq. (32).

propagates in the computational domain. For cases with the buffer zone, the wave is attenuated. In Fig. 10, a shift associated with the uniform mean flow velocity in the computational domain is clearly visible. For the mean flow velocity given by a sine function and Eq. (32), the shift is non-uniform, as can be seen in Figs 11 and 12.
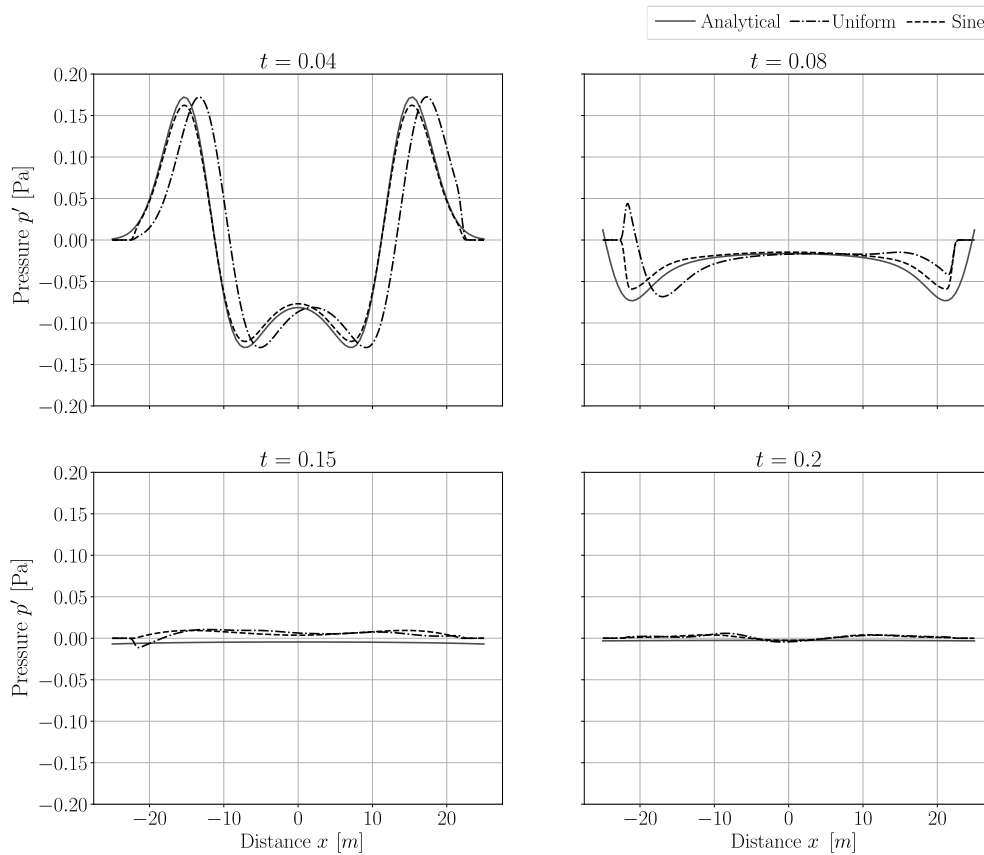

Fig. 9. Distribution of pressure along x axis for $y = 0$ for simulations of two-dimensional impulse (with presence of the mean flow).
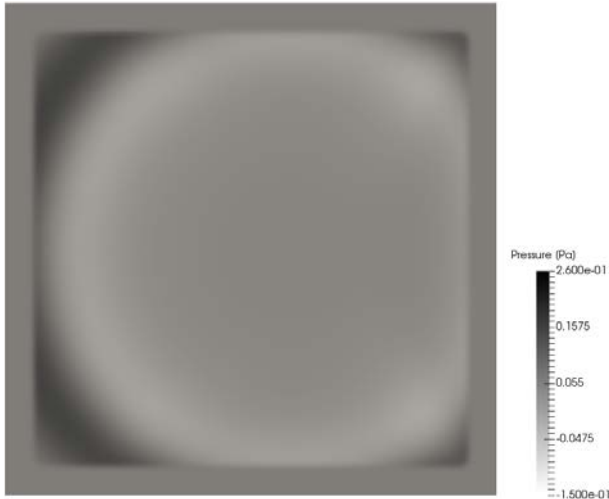
Fig. 10. Distribution of pressure for two-dimensional model with a uniform mean flow in x direction and the buffer zone for time $t = 0.08$ s.
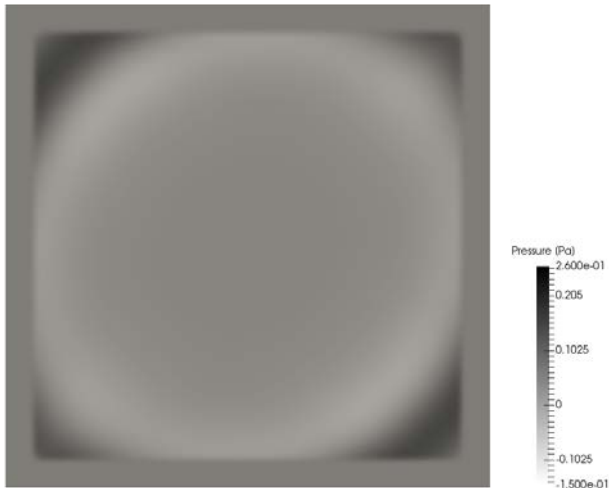

Fig. 11. Distribution of pressure for two-dimensional model with a mean flow given by Eq. (32) and the buffer zone for time $t = 0.08$ s.
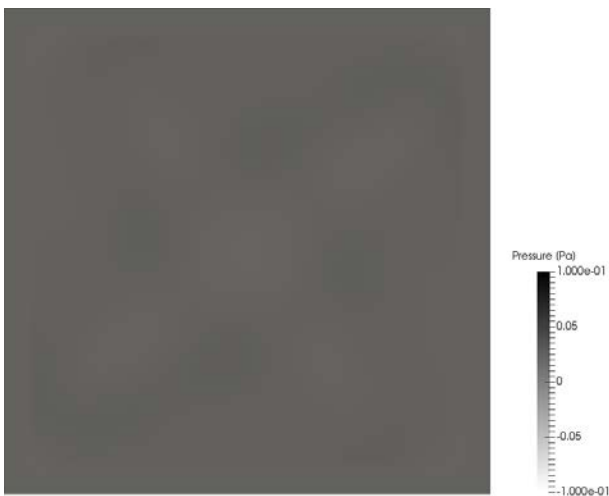

Fig. 12. Distribution of pressure for two-dimensional model with a mean flow given by Eq. (32) and the buffer zone for time $t = 0.2$ s.

3.3. Oscillating cylinder

Another two-dimensional case tested and verified in this paper was propagation of the acoustic wave generated by a radially oscillating cylinder. Oscillations of pressure at the surface of the cylinder are described by the equation:

$$p'(t) = p_0 \sin(2\pi f t), \qquad (33)$$

where p_0 is the amplitude of pressure, f is the frequency.

A round surface around the cylinder was adopted as a computational domain. Because the whole surface oscillates with the same frequency, it was assumed that the model is symmetrical and only half of the surface was modelled. This was shown in the Fig. 13. Computational domain dimensions equal to $a = 4$ m, $r = 30$ m were adopted. The time step was equal to $\Delta t = 1 \cdot 10^{-5}$. The coefficients in Eq. (33) were equal to $p_0 = 0.05$ MPa, $f = 500$ Hz.
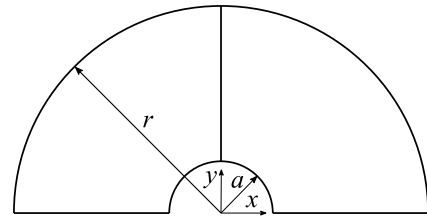

Fig. 13. Model of the computational domain for oscillating cylinder simulations.

Analytical solution of this problem is given by (SUDER-DĘBSKA et al., 2018):

$$p'(r,t) = -j\omega\rho\frac{v_0}{kH_0'(ka)}H_0(kr)e^{j\omega t}, \qquad (34)$$

where j is the imaginary unit, $\omega = 2\pi f$ is the angular frequency, v_0 is the velocity of oscillations, $k = \omega/c$ is the wavenumber, H_0 is the Hankel function of the first kind, H_0' is the derivative of Hankel function with respect to r.

The results of the simulations are shown in Figs 14 and 15. Figure 14 shows the pressure field after time of simulation $t = 0.085$ s. It can be seen that for given
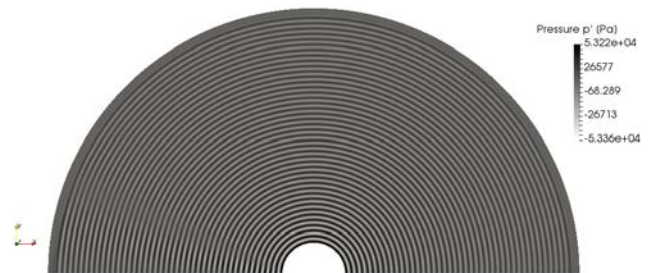

Fig. 14. Pressure field for two-dimensional oscillating cylinder simulations.
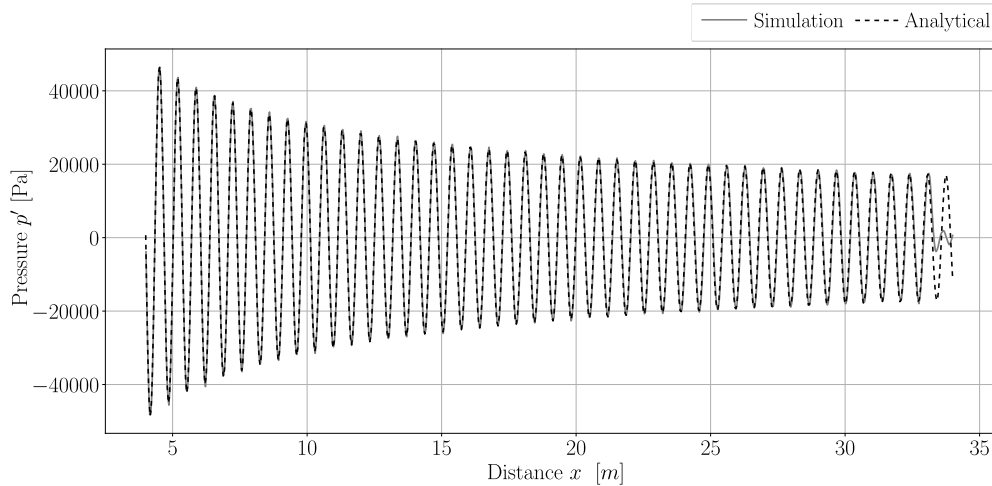
Fig. 15. Distribution of pressure along y axis for $x = 0$ at $t = 0.085$ s.

distance from source r, the value of pressure is uniform regardless of the angle θ.

In Fig. 15 distribution of pressure along y axis for $x = 0$ at $t = 0.085$ s, for both simulation results and analytical calculations given by Eq. (34) is shown. The behaviour of the acoustic wave is very similar in both cases.

3.4. Backward-facing step

The last analysed case was backward-facing step, a well known benchmark case for CFD simulations. This model was chosen because of its universality and the possibility of its use in modelling of many phenomena (Armaly *et al.*, 1983; Le *et al.*, 1997; Biswas *et al.*, 2004). Two versions of this case were analysed and compared, with and without the mean flow. Firstly, the velocity and pressure distributions of the flow over the backward-facing step were computed using Navier-Stokes equations implemented in FEniCS library (Langtangen, Logg, 2017). The result, the velocity field, was imported into acoustic simulations as variables (U, V), which describe the mean velocity field. Then, the developed tool was used to calculate the wave propagation. The geometric model is shown in the Fig. 16, which also shows the boundaries used in modelling.

The boundary conditions for each of the models (Navier-Stokes, linearised Euler equations) are shown in Table 4. If the variable is not specified in the ta-
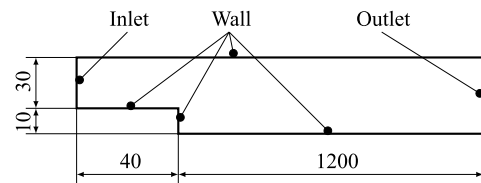

Fig. 16. Geometric model of backward-facing step (dimensions in mm).

ble, its boundary condition was equal to zero gradient of the variable on that boundary – $\partial v / \partial n = 0$ or $\partial p / \partial n = 0$. In the flow simulations, two different velocity profiles were given at the inlet, described by the equations in the table. The maximum velocity values were 3.6 and 10 m/s.

The results of the flow simulations using Navier-Stokes equations, for inlet velocity profiles given in Table 4 were shown in Figs 17 and 18. For these simulations, the time step size was changed depending on the velocity at inlet.

Then, the calculated velocity profiles were used in LEE simulations as the mean flow velocity. This required the development of a read/write tool that FEniCS does not have by default. As mentioned in Table 4, in the wave propagation simulation, the velocity was given by a time-dependent sine function for the frequency equal to $f = 500$ Hz. The buffer zone boundary condition was added at the outlet. It was placed on the entire height of the domain ($y = 0$–0.4) and for

Table 4. Boundary conditions for flow (NS) and acoustic wave propagation (LEE) simulations (p, v are the flow variables, p', v' are the acoustic variables).

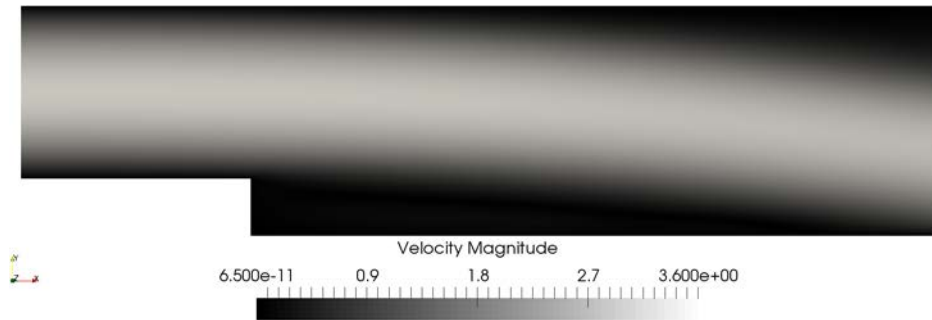| Boundary	NS model	LEE model
Inlet	$v = (160; 444.445)(y - 0.1)(0.4 - y)$ m/s	$v' = 0.01 \sin(500 \cdot 2\pi t)$ m/s
Wall	$v = 0$ m/s	$v' = 0$ m/s
Outlet	$p = 0$ Pa	$p' = 0$ Pa

Fig. 17. Velocity distribution of flow over backward-facing step for maximum velocity at inlet equal to $u_{\max}$ = 3.6 m/s.
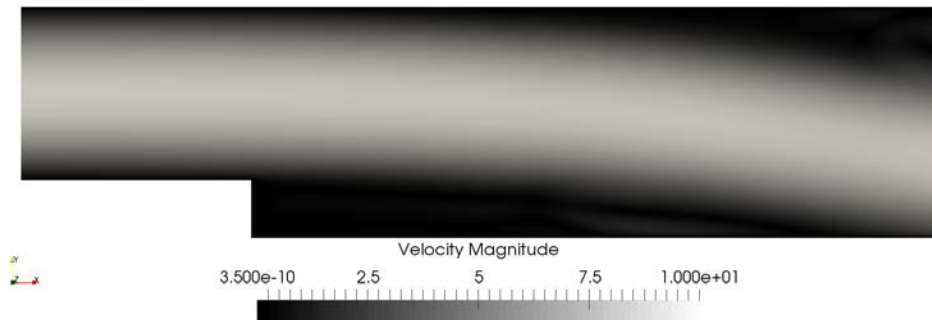

Fig. 18. Velocity distribution of flow over backward-facing step for maximum velocity at inlet equal to $u_{\max}$ = 10 m/s.
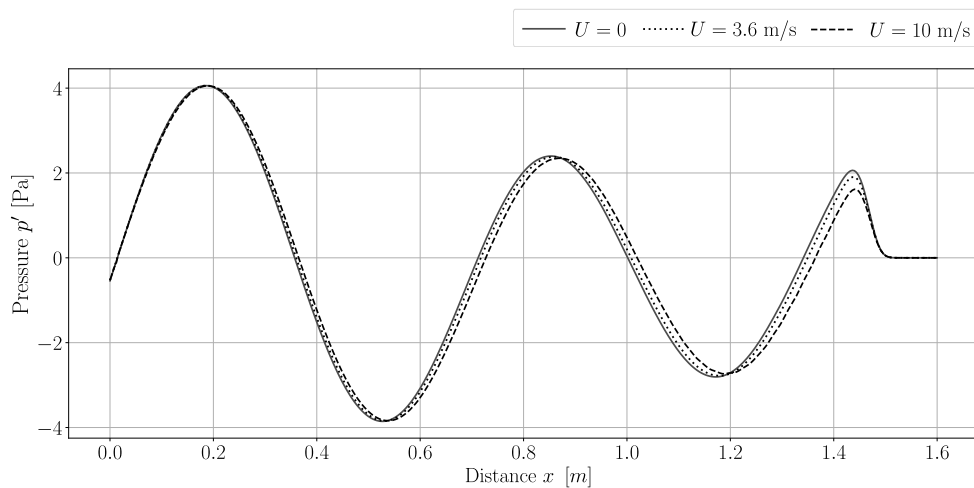

Fig. 19. Pressure values for linearised Euler simulations of wave propagation over backward-facing step, with and without mean flow.

x = 1.5–1.6. In these simulations, the time step size was equal to $\Delta t = 5 \cdot 10^{-7}$. The results were shown in Fig. 19.

In the figure, the values of pressure for different mean flow velocities are shown. The data sampled along x axis and for $y = 0.25$ are shown. It can be seen that the distributions computed with the mean flow presence are shifted relative to the distribution calculated without the flow. This agrees with the assumptions and confirms the correctness of the developed model and tool. In addition, the effect of the damping zone can be seen in the graph. The wave was fully absorbed and no reflection occurred.

4. Conclusions

This paper presents implementation and verification of a finite element numerical model of linearised Euler equations which describe the acoustic wave propagation. The developed solver can be used to model the propagation in the unbounded domains due to implemented non-reflective boundary conditions called buffer zone. The proposed solver is able to take the mean flow velocity into account and can be used to model a one-way flow-acoustic coupling.

The solver was used to solve one and two-dimensional cases, to verify and validate the performance

of the model. The performance of the non-reflective boundary condition was also examined. The numerical results were compared to the analytical solutions, they were simiar, which indicates that the model has been correctly implemented.

The proposed model was used to solve the case of the acoustic wave propagation over a backward-facing step in the presence of the flow.

The FEniCS software used for solving the equations is proven to be a versatile tool. The developed code is easily scalable and can be used both on a personal computer and HPC cluster.

The developed tool suffers from problems similar to other finite element solvers and mesh methods in general – the need to use a properly dense computational grid and a small time step to solve the equations with the least possible error.

Despite this, both the tool and the results obtained using it are promising. The tool could be used to model the wave propagation in waveguides and mufflers, but as for today it requires further development and testing, especially for 3D cases and parallel computations.

Acknowledgements

References

1. Åbom M. (2006), *An Introduction to Flow Acoustics*, Stockholm, Sweden: KTH.

2. Ahrens J., Geveci B., Law C. (2005), Paraview: An end-user tool for large data visualization, [in:] Hansen C.D., Johnson C.R. [Eds], *Visualization Handbook*, Butterworth-Heinemann, pp. 717–731, doi: 10.1016/ B978-012387582-2/50038-1.

3. Alnaes M.S. *et al.* (2015), The Fenics project version 1.5, *Archive of Numerical Software*, **3**(100): 9–23, doi: 10.11588/ans.2015.100.20553.

4. Armaly B.F., Durst F., Pereira J.C.F., Schonung B. (1983), Experimental and theoretical investigation for backward-facing step flow, *Journal of Fluid Mechanics*, **127**: 473–496, doi: 10.1017/ S0022112083002839.

5. Atkins H., Casper J. (1994), Nonreflective boundary conditions for high-order methods, *AIAA Journal*, **32**(4): 512–518, doi: 10.2514/3.12015.

6. Bailly C., Juve D. (2000), Numerical solution of acoustic propagation problems using linearized Euler equations, *AIAA Journal*, **38**(1): 22–29, doi: 10.2514/2.949

7. Bendat J.S., Piersol A.G. (2010), *Random Data. Analysis and Measurement Procedures*, Hoboken, US: John Wiley & Sons, Inc.

8. Berenger J.-P. (1994), A perfectly matched layer for the absorption of electromagnetic waves, *Journal of Computational Physics*, **114**(2): 185–200, doi: 10.1006/jcph.1994.1159

9. Bermudez A., Hervella-Nieto A., Prieto A., Rodriguez R. (2008), Perfectly matched layers, [in:] *Computational Acoustics of Noise Propagation in Fluids – Finite and Boundary Element Methods*, pp. 167–196, Springer: Berlin–Heidelberg, doi: 10.1007/978-3-540-77448-8_7.

10. Biswas G., Breuer M., Durst F. (2004), Backward-facing step flows for various expansion ratios at low and moderate Reynolds numbers, *Journal of Fluids Engineering*, **126**(3): 362–374, doi: 10.1115/1.1760532.

11. Butcher J.C. (2016), *Numerical Methods for Ordinary Differential Equations*, Chichester, England: John Wiley & Sons Inc., doi: 10.1002/9781119121534.

12. Colonius T. (1997), *Lectures on Computational Aeroacoustics*, Pasadena, United States: California Institute of Technology.

13. Czajka I., Gołas A. (2017), *Engineering Methods of Numerical Analysis and Design of Experiment* [in Polish], Kraków, Poland: Wydawnictwa AGH.

14. Dykas S., Wroblewski W. (2006), *Method of Modeling Aerodynamic Noise in Transonic Flows* [in Polish], Gliwice, Poland: Wydawnictwo Politechniki Śląskiej.

15. Dykas S., Wroblewski W., Rulik S., Chmielniak T. (2010), Numerical method for modeling of acoustic waves propagation, *Archives of Acoustics*, **35**(1): 35–48, doi: 10.2478/v10168-010-0003-7.

16. Epikhin A., Evdokimov I., Kraposhin M., Kalugin M., Strijhak S. (2015), Development of a dynamic library for computational aeroacoustics applications using the OpenFOAM open source package, *Procedia Computer Science*, **66**: 150–157, doi: 10.1016/ j.procs.2015.11.018.

17. Ewert R., Schröder W. (2003), Acoustic perturbation equations based on flow decomposition via source filtering, *Journal of Computational Physics*, **188**(2): 365–398, doi: 10.1016/s0021-9991(03)00168-2.

18. Giles M.B. (1990), Nonreflecting boundary conditions for Euler equation calculations, *AIAA Journal*, **28**(12): 2050–2058, doi: 10.2514/3.10521.

19. Gill J., Fattah R., Zhang X. (2017), Towards an effective non-reflective boundary condition for computational aeroacoustics, *Journal of Sound and Vibration*, **392**: 217–231, doi: 10.1016/j.jsv.2016.11.036

20. Givoli D. (2008), Computational absorbing boundaries, [in:] *Computational Acoustics of Noise Propagation in Fluids – Finite and Boundary Element Methods*, Berlin–Heidelberg: Springer, doi: 10.1007/978-3-540-77448-86.

21. Hagstrom T., Goodrich J. (2003), Accurate radiation boundary conditions for the linearized Euler

equations in Cartesian domains, *SIAM Journal on Scientific Computing*, **24**(3): 770–795, doi: 10.1137/s1064827501395914.

22. KALTENBACHER M. (2017), Fundamental equations of acoustics, [in:] Kaltenbacher M. (Ed.), *Computational Acoustics. CISM International Centre for Mechanical Sciences (Courses and Lectures)*, Vol. 579, pp. 1–33, Springer, Cham, doi: 10.1007/978-3-319-59038-7_1.

23. KOLOSZÁR L., VILLEDIEU N., DECONINCK H., RAMBAUD P., ANTHOINE J. (2019), Improved characteristic non-reflecting boundary conditions for the linearized Euler equations, [in:] *16th AIAA/CEAS Aeroacoustics Conference*, doi: 10.2514/6.2010-3984.

24. KOSLOFF R., KOSLOFF D. (1986), Absorbing boundaries for wave propagation problems, *Journal of Computational Physics*, **63**(2): 363–376, doi: 10.1016/0021-9991(86)90199-3.

25. KUTTRUFF H. (2007), *Acoustics. An introduction*, Abingdon, England: Taylor & Francis.

26. LANGTANGEN H.P., LOGG A. (2017), *Solving PDEs in Python – The FEniCS tutorial*. Vol. I. Cham, Switzerland: Springer, doi: 10.1007/978-3-319-52462-7.

27. LE H., MOIN P., KIM J. (1997), Direct numerical simulation of turbulent flow over a backwardfacing step, *Journal of Fluid Mechanics*, **330**: 349–374, doi: 10.1017/ S0022112096003941.

28. LIGHTHILL M.J. (1952), On sound generated aerodynamically. I. General theory, *Proceedings of the Royal Society of London. Series A. Mathematical and Physical Sciences*, **211**(1107): 564–587, doi: 10.1098/rspa.1952.0060.

29. LOGG A., MARDAL K.A., WELLS G. [Eds], (2012), *Automated solution of differential equations by the finite element method. The FEniCS book, Lecture Notes in Computational Science and Engineering*, Berlin–Heidelberg: Springer, doi: 10.1007/978-3-642-23099-8.

30. LYRINTZIS A.S., GEORGE A.R. (1989), Use of the Kirchhoff method in acoustics, *AIAA Journal*, **27**(10): 1451–1453, doi: 10.2514/3.10285.

31. ŁOJEK P., CZAJKA I. (2019), Scalable finite element implementation of linearized Euler equations, [in:] *XXIII Conference on Acoustic and Biomedical Engineering*.

32. MECHEL F.P. [Ed.] (2008), *Formulas of Acoustics*, Heidelberg, Germany: Springer-Verlag GmbH, doi: 10.1007/978-3-662-07296-7.

33. POVITSKY A. (2000), *Numerical study of wave propagation in a non-uniform flow*, Technical Report, Institute for Computer Applications in Science and Engineering, NASA Langley Research Center.

34. RIBES A., CAREMOLI C. (2007), Salomé platform component model for numerical simulation, [in:] *Compsac 07: Proceeding of the 31st Annual International Computer Software and Applications Conference (COMPSAC 2007)*, Beijing, 2007, pp. 553–564, doi: 10.1109/COMPSAC.2007.185.

35. RICHARDS S.K., ZHANG X., CHEN X.X., NELSON P.A. (2004), The evaluation of non-reflecting boundary conditions for duct acoustic computation, *Journal of Sound and Vibration*, **270**(3): 539–557, doi: 10.1016/j.jsv.2003.09.042.

36. RIENSTRA S.W., HIRSCHBERG A. (2004), *An Introduction to Acoustics*, Eindhoven University of Technology, Eindhoven, Netherlands.

37. SUDER-DEBSKA K., GOŁAS A., FILIPEK R. (2018), *An Introduction to Applied Acoustics* [in Polish], Kraków, Poland: Wydawnictwa AGH.

38. WAGNER C.A., HUTTL T., SAGAUT P. [Eds] (2006), *Large-Eddy Simulation for Acoustics*, New York, US: Cambridge University Press, doi: 10.1017/CBO9780511546143.